

A MULTIWAVELENGTH STUDY OF DISTANT BLAZAR PKS 0537-286

N.SAHAKYAN^{1,2}, D.ISRAYELYAN¹, G.HARUTYUNYAN¹

Received 13 February 2020

Accepted 26 August 2020

We report the results of broadband observations of distant blazar PKS 0537-286 ($z=3.1$) using data spanning more than ten years from the Fermi Large Area Telescope together with Swift UVOT/XRT archival data taken between 2005 and 2017. In the γ -ray band, the peak flux above 100 MeV, $F_\gamma = (6.23 \pm 0.56) \cdot 10^{-7}$ photon $\text{cm}^{-2} \text{s}^{-1}$ observed on MJD 57874 within one week, corresponds to $L_\gamma = 2.46 \cdot 10^{49}$ erg s^{-1} isotropic γ -ray luminosity. The Swift XRT data analyses show that the X-ray emission is characterized by a significantly hard photon index, $\Gamma_{\text{X-ray}} \leq 1.3$, and an X-ray flux of $4 \cdot 10^{-12}$ erg $\text{cm}^{-2} \text{s}^{-1}$, which is almost constant over twelve years. The spectral energy distribution is modeled within one-zone leptonic models assuming the emission region is within the broad-line region. The observed X-ray and γ -ray data are modeled as inverse Compton scattering of (i) only synchrotron photons and (ii) synchrotron and external photons on the electron population that produces the radio-to-optical emission. The modeling shows that the nonthermal electrons in the jet of PKS 0537-286 have a hard power-law index (<1.9) and that the jet should be particle dominated with a luminosity within 10^{45} - 10^{46} erg s^{-1} .

Keywords: *PKS 0537-286: γ -rays: blazars*

1. Introduction. The recent observations in the High Energy γ -ray band (HE >100 MeV) show that the extragalactic γ -ray sky is dominated by the emission from Active Galactic Nuclei (AGN) of different types [1]. Interestingly, the γ -ray emission was observed not only from the most extreme subclass of AGNs (blazars) but also from radio galaxies [2-5] and Seyfert galaxies [6]. This provides an exceptional chance to investigate the relativistic processes under different conditions.

In the unification scheme of AGNs [7], blazars are a subclass of AGNs with relativistic jets oriented close to our line of sight. Blazars are known to emit electromagnetic emission ranging from radio to very high energy γ -ray bands (VHE >100 GeV) which is characterized by high amplitude and short time scale variability. The most extreme time scale variability is observed in the HE and VHE γ -ray bands when the flux amplification time scale can be as short as minute scales (e.g., [8-10]). Depending on the emission line properties, blazars are usually sub-grouped into flat spectrum radio quasars (FSRQs) and BL Lac objects, where BL Lacs have no or weak emission lines, while in FSRQs the emission lines are stronger and quasar-like [7]. Blazars being powerful sources were

always considered as effective neutrino emitters. This association was strengthened by the recent association of TXS 0506+056 with the neutrino event IceCube-170922A [11-13] which opened new perspectives for studying blazars, using multimessenger data (e.g., [14-18]).

The blazar spectral energy distribution (SED) is characterized by two broad peaks of which the lower energy (IR/optical/UV/) one is due to the synchrotron emission of electrons in the jet while the origin of the second peak (at HE γ -ray band) is unknown. It is commonly described by inverse Compton scattering of the synchrotron photons or photons external to the jet (e.g., for the modeling of the SED of several well-known blazars see [19-22]). The exact nature of the photon fields depends on the localization of the emission region, which is unknown [23].

Due to the small inclination angle and large bulk motion, the emission from blazars is significantly amplified by relativistic beaming because of which the blazars are observed even at very high redshifts. For example, in the fourth catalog of AGNs detected by the Fermi Large Area Telescope (Fermi-LAT), the most distant blazar observed to date is GB 1508+5714 at $z = 4.1$ [24]. At this distance, the source should be extremely powerful and extremely efficient to emit detectable electromagnetic flux. These objects typically host a black hole with a mass of $> 10^9 M_{\odot}$, so it is important to investigate them to understand the extreme environments around supermassive black holes. Also for the high redshift blazars, the produced γ -rays during their propagation can be absorbed due to the interaction with the extragalactic background light (EBL) photons, so the observed flux could help measure the density of EBL. So the distant blazars are ideal targets not only for studying the physical processes in the extreme conditions but also for understanding the structure and evolution of the Universe.

PKS 0537-286, at $z = 3.104$, is a luminous blazar included in the fourth catalog of AGNs detected by Fermi-LAT. It has been frequently observed in the X-ray band with various instruments (ASCA [25], ROSAT [26], XMM [27]) which showed that it is a very bright source with a luminosity of $L_{x\text{-ray}} = 10^{47} \text{ erg s}^{-1}$ between 0.1-1 keV. Considering multiple observations of PKS 0537-286 with the Neil Gehrels Swift observatory (Swift) carried out between 2005 and 2017 which provide data in both optical/UV and X-ray bands as well as more than ten years of data in the γ -ray band accumulated by Fermi-LAT, PKS 0537-286 has become an ideal object for exploring the physics of distant blazars. This motivated us to look at the origin of the multiwavelength emission from PKS 0537-286 from a new standpoint.

The paper is structured as follows. The results of the X-ray and γ -ray data analyses are presented in Section 2. The modeling of broadband SED is discussed in Section 3. Discussion and conclusions are presented in Section 4.

2. *Multiwavelength Observations and data analysis.* The observation of blazars in the multiwavelength bands provides information not only on their emission properties in the single bands but also are crucial for understanding the physics of jets through the theoretical modeling of the observed data. In this paper, the origin of the multiwavelength emission from PKS 0537-286 is studied by analyzing Swift UVOT/XRT and Fermi-LAT data.

2.1. *Swift telescope observations of PKS 0537-286.* Swift [28] observed PKS 0537-286 16 times between 2005 and 2017. All UVOT and XRT data, except ObsidID 30816011 with an extremely short exposure (159.4sec), were extracted and analyzed. The XRT exposures range from 0.11 ks (ObsID 30816011) to 14.87 ks (ObsID 35240002), and all the observations were made in the photon counting mode and no evidence of pile-up was found. The XRT data were first calibrated and cleaned with standard filtering criteria using the most recent calibration databases with the *xrtpipeline* software module distributed with the XRT Data Analysis Software (version v3.5.0). Events for the spectral analysis were selected within a 20-pixel (47") circle with the source at the center, while the background region had an annulus with the same center and inner and outer radii of 51 (120") and 85 pixels (200"), respectively. As the count rate in most of the observations was low, the Cash statistics [29] on ungrouped data was used. Spectral analysis was performed using XSPEC version 12.10.1. The spectra were fitted with an absorbed power-law model in the energy range from 0.3 keV to 10 keV with a neutral hydrogen column density fixed to its Galactic value of $N_{\text{H}} = 2.22 \cdot 10^{20} \text{ cm}^{-2}$. The results are given in Table 1 where for each observation, the ObsidID, date, exposure, photon index Γ , flux and C-stat/d.o.f. are provided. The X-ray flux (0.3-10 keV) varies in the narrow range of $F = (3.01 - 4.58) \cdot 10^{-12} \text{ erg cm}^{-2} \text{ s}^{-1}$ being almost constant during the twelve years of observation of PKS 0537-286. Interestingly, the X-ray emission is characterized by a substantially hard photon index of < 1.3 which implies that in νF_{ν} representation the X-ray spectrum has an increasing shape.

Considering only the observations with counts > 100 , which allow confidential estimation of the parameters, the hardest photon index is 1.03 ± 0.19 observed on May 12, 2017.

The data from the Swift UVOT observations were used to estimate the fluxes of the source in the optical and UV bands. The UVOT observation takes data in six bands, UVW2 (188 nm), UVM2 (217 nm), UVW1 (251 nm), U (345 nm), B (439 nm) and V (544 nm). The source counts were extracted from an aperture of 5".0 radius around the source. The background counts were taken from the neighboring circular region having a radius of 20" located close to the source region and not being contaminated with any signal from the nearby sources. *Uvotsource* tool was used to convert the source counts into fluxes using the conversion factors

Table 1

FITTING RESULTS OF THE DATA OBTAINED BY THE XRT
INSTRUMENT ON BOARD SWIFT

Obs. ID	Date	Exp. Time (s)	Γ^a	Flux ^b	C_{stat} (d.o.f.)
30816001	Oct 27, 2006	3040	1.09 ± 0.17	4.18 ± 0.74	1.07 (156)
30816003	Oct 30, 2006	3894	1.33 ± 0.13	4.09 ± 0.55	1.12 (197)
30816004	Oct 31, 2006	4425	1.27 ± 0.14	3.62 ± 0.50	0.97 (201)
30816005	Feb 10, 2008	6708	1.10 ± 0.11	4.58 ± 0.42	1.23 (278)
30816006	Feb 12, 2008	5274	1.01 ± 0.13	4.14 ± 0.57	1.11 (226)
30816007	Feb 14, 2008	4822	1.11 ± 0.13	4.16 ± 0.57	1.14 (215)
30816008	Oct 07, 2008	1593	1.04 ± 0.29	3.29 ± 0.98	0.68 (65)
30816009	Mar 12, 2010	1076	1.00 ± 0.34	3.82 ± 1.34	0.91(51)
30816010	Mar 12, 2010	2018	0.93 ± 0.32	2.07 ± 0.69	1.28(49)
30816012	Sep 06, 2011	3931	1.06 ± 0.18	3.01 ± 0.57	0.86(135)
35240001	Nov 23, 2005	9038	1.17 ± 0.10	3.51 ± 0.37	0.87(306)
35240002	Dec 8, 2005	14750	1.13 ± 0.08	3.84 ± 0.40	1.08(407)
36783001	May 17, 2007	5414	1.32 ± 0.11	4.20 ± 0.48	1.12(257)
36783002	May 10, 2017	1933	1.28 ± 0.20	4.28 ± 0.87	1.09(116)
36783003	May 12, 2017	2238	1.03 ± 0.19	4.52 ± 0.91	0.98(123)
Swift UVOT					
	U	W1	M2	B	V
30816008	20.8 ± 1.2	21.5 ± 1.8	21.9 ± 4.4	19.7 ± 0.4	19.3 ± 0.6
30816009	21.0 ± 1.0	20.2 ± 0.5	21.0 ± 0.9	20.0 ± 0.3	18.7 ± 0.3
35240002	20.8 ± 0.1	22.0 ± 2.1	21.3 ± 1.1	19.5 ± 0.3	18.8 ± 0.3

Notes: ^a Photon index from X-ray data analysis. ^b X-ray flux in the energy range 0.3-10 keV in units of $\times 10^{-12}$ erg cm^{-2} s^{-1} (corrected for the Galactic absorption).

provided in [30]. The data were corrected for dust contamination using the reddening coefficient $E(B - V)$ from the infrared science archive¹. Initially, all observations were processed and no variability in a single filter was found. For most of the observations, in several filters, the counts were not enough to measure the source magnitude and only for ObsidIDs 30816008, 30816009 and 3524002 five filters were available. The Swift UVOT observations of PKS 0537-286 in magnitudes for these ObsidIDs are given below Table 1 (last lines).

2.2. Fermi LAT observations of PKS 0537-286. Fermi-LAT is a pair conversation telescope sensitive to the photons in the energy range from 100 MeV to 300 GeV [31]. Launched on June 11, 2008, it is always on survey mode since August 2008 and scans the entire sky every three hours, providing the deepest view of the HE γ -ray sky.

¹ <https://irsa.ipac.caltech.edu/applications/DUST/>

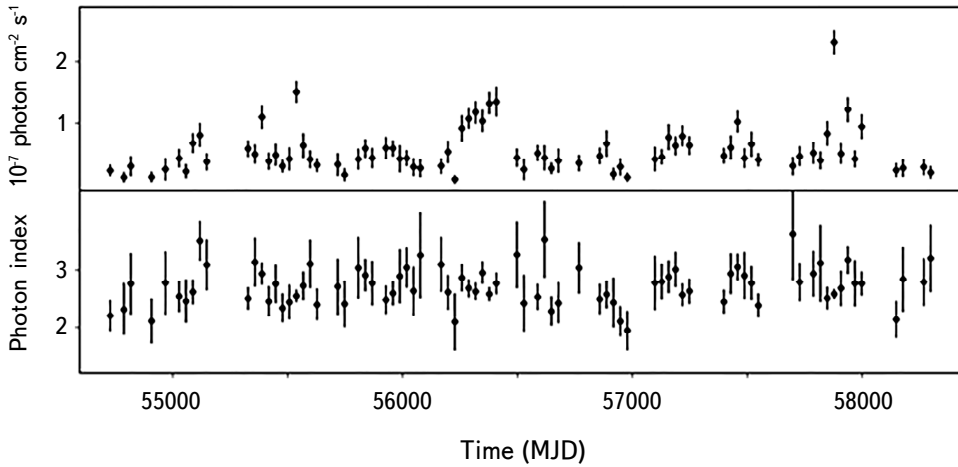


Fig.1. The γ -ray light curve and the photon index. The light curves were calculated using 30-day bins. For clarity, the periods with the upper limits are not shown.

In this paper, the publicly available Fermi-LAT data accumulated from 4th August 2008 to 4th August 2018 (ten years) were downloaded and analyzed. The past 8 events in the energy range from 100 MeV to 500 GeV with the highest probability of being photons ("event class=128" and "evtype=3") were analyzed with the Fermi Sciences Tools 1.2.1 software package. The photons from the 12° region centered on the γ -ray position of PKS 0537-286 (RA, Dec)=(84.99, -28.66) were downloaded and binned into a $16^\circ.9 \times 16^\circ.9$ square region of interest (ROI) with a stereographic projection into pixels of $0^\circ.1 \times 0^\circ.1$ and into 35 equal logarithmically-spaced energy bins using *gbin* tool. The standard binned likelihood analysis was performed following the recommendation by Fermi-LAT collaboration, and the results were compared by performing the same analysis using *Fermipy* and *Enrico* python packages. The fitting model includes diffuse emission components and γ -ray sources within ROI (the model file is created based on the most recent 4FGL [1]). The Galactic and isotropic γ -ray backgrounds were modeled using the standard *gll_iem_v06* and *iso_P8R2_SOURCE_V6_v06 models*. During the fit, the normalization of background models, as well as fluxes and spectral indices of the sources within ROI, are left as free parameters.

The time-averaged γ -ray spectrum of PKS 0537-286 was first modeled using a log-parabola [32] as in 4FGL then assuming a power-law shape. The latter will be used in the light-curve and the SED calculations. As when shorter periods or narrow energy intervals are used a power-law can be a good approximation of the spectrum. When log-parabola is considered, the spectrum of PKS 0537-286 is best described when $\alpha = 2.70 \pm 0.03$ and $\beta = 0.09 \pm 0.03$ with the corresponding integral flux of $F_\gamma = (4.19 \pm 0.15) \cdot 10^{-8}$ photon $\text{cm}^{-2} \text{s}^{-1}$. The Test Statistics (TS), $TS = 2(\log L - \log L_0)$,

where L and L_0 are the likelihoods with or without the source, is $TS=1824.5$ above 100 MeV, corresponding to a $\approx 42.7\sigma$ detection significance. The γ -ray flux of PKS 0537-286 is impressive when considering its distance ($z=3.1$). The spectral parameters, when the power-law model is considered, are $F_\gamma = (4.40 \pm 0.19) \cdot 10^{-8}$ photon $\text{cm}^{-2} \text{s}^{-1}$ and $\Gamma = 2.73 \pm 0.03$. This power-law model was used to compute the spectrum of PKS 0537-286 by separately running *glike* for 6 energy bands (Fig.2).

The γ -ray flux and photon evolution in time were investigated by generating the light curves using the unbinned likelihood analysis method implemented in the *glike* tool. The flux and photon index were measured in each time interval, restricting the energy range to (0.1-300) GeV and assuming a power-law spectrum for PKS 0537-286. To reduce the uncertainties in the estimations, the photon indices of all background sources (except PKS 0537-286) are fixed to the best guess values obtained in the analysis of the entire 10 years of data. Since no variability is expected for the background diffuse emission, the normalization of both background components is also fixed to the values obtained for the whole period.

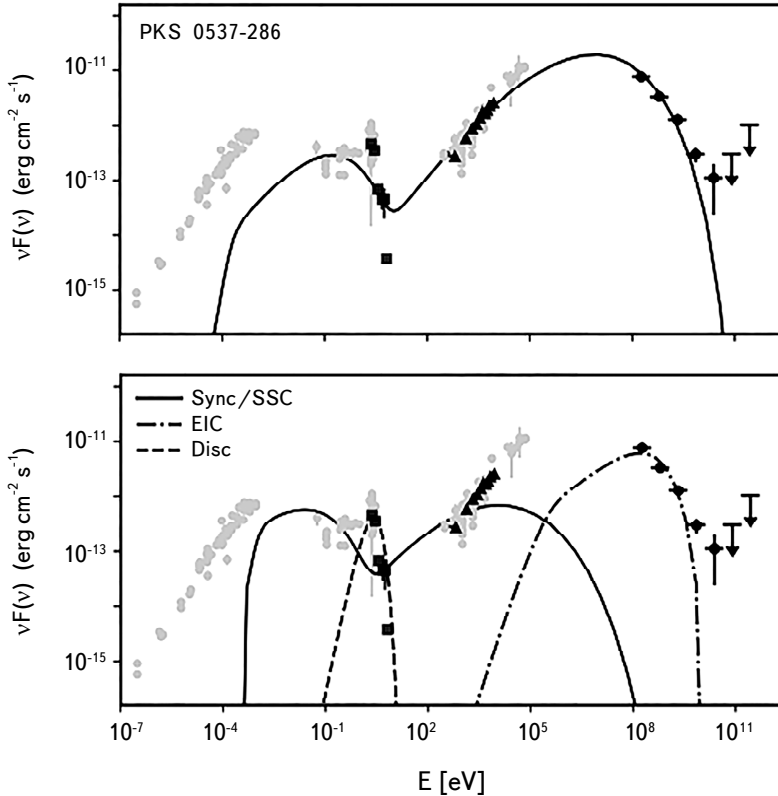


Fig.2. The broadband SED of PKS 0537-286. Upper panel: The modeling considering only the SSC model. Lower panel: The modeling considering both synchrotron (SSC) and external photons (EIC).

Initially, the light curves were generated using a 7-day time binning. There is clear evidence of flux variation in short time scales, although in many periods only upper limits $TS < 16$ are derived. The highest flux measured in week scale is $(6.23 \pm 0.56) \cdot 10^{-7}$ photon $\text{cm}^{-2} \text{s}^{-1}$, which nearly 15 times exceeds the average flux reported above. This flux was observed during the major flare that occurred around MJD 57874. However, the light curve contains a large number of periods with only upper limits, which prevents the detailed study of the variability in short time scales. For a more quantitative investigation of the evolution of the γ -ray flux in time, the light curve is generated with a month time binning (Fig.1). Again, a clear indication of flux variability is evident with several times when the flux was above 10^{-7} photon $\text{cm}^{-2} \text{s}^{-1}$. One of such periods starts from MJD 56272 and lasts for 30 days. The highest flux corresponds to $(2.32 \pm 0.19) \cdot 10^{-7}$ photon $\text{cm}^{-2} \text{s}^{-1}$ observed during the major flare mentioned above. The photon index does not show significant changes, most of the time it varying in the range of >2.5 . These analyses show that the γ -ray emission from PKS 0537-286 is variable in both short and long time scales.

3. *Broadband SEDs.* The broadband observations of blazars are unique tools to explore their physics. The data ranging from radio to VHE γ -ray band can allow to probe the physical processes at large energy intervals and to estimate several important parameters of the jet. The multiwavelength archival data from the observation of PKS 0537-286 are shown in Fig.2 with gray color. As has been discussed in the previous section, there is no variability in the X-ray band and the data are not enough for searching variability in the optical/UV bands. To increase the statistics, all the Swift observations were merged and analyzed which provides the fluxes in the mentioned bands. These data are shown in Fig.2 with squares and triangles respectively. Since there are no simultaneous multiwavelength data available for testing PKS 0537-286 jet physics in different periods, and as the main purpose of the current paper is to estimate the main parameters of the jet of PKS 0537-286 in the average state, even if the γ -ray emission varies in some periods, the γ -ray flux averaged over 10 years of observations was used in the modeling (black circles in Fig.2).

3.1. *Modeling of the SED.* The SED shown in Fig.2 has a typical double-peaked structure. The low-energy peak (from radio to optical/UV) is most likely due to the non-thermal synchrotron emission of relativistic electrons, while the second component can be produced from the Inverse Compton (IC) scattering of low energy synchrotron photons (Synchrotron Self Compton; SSC) [33-35] or scattering of photons external to the jet (External Compton (EIC)). The external photon field can be either the photons reflected by Broad Line Region (BLR) clouds [36] or by photons from a dusty torus [37,38]. Domination of one of the components mostly depends on the localization of the emitting region, which is

unknown. Thus, in the modeling, both photons fields are considered for modeling the HE component in the SED of PKS 0537-286.

In the modeling, it is assumed that the multiwavelength emission is produced in a single zone (one-zone scenarios). The emission region is a spherical blob moving relativistically along the jet with a bulk Lorentz factor of Γ_{jet} . The produced emission will be Doppler boosted with $\delta = \Gamma_{\text{jet}}(1 - \beta \cos \theta)^{-1}$, where θ is the angle between the direction of observation and the axis of the jet. In this work, we assume $\delta = 20$, which is typical for the bright blazars. The blob has tangled magnetic field with the magnitude of B and it is filled with nonthermal electrons which have a power-law with exponential cut-off distribution given by

$$N_e(\gamma_e) = N_0(\gamma_e)^{-\alpha} \exp[-\gamma_e/\gamma_{\text{cut}}] \quad (1)$$

between γ_{min} and γ_{max} , and N_0 defines the total energy of the electrons U_e . The electrons with the energy distribution given by Eq. (1), under the magnetic field will produce synchrotron emission which can explain the observed low energy component.

The produced synchrotron photons can serve as the target photon field for the IC scattering. In addition to these photons, it is assumed, that the emission region is within the broad BLR and the disc photons reflected from the BLR clouds can also be IC up-scattered and explain the observed HE component. The density of the BLR photons, $u_{\text{BLR}} = \tau L_{\text{disc}} / 4\pi R_{\text{BLR}}^2$, depends on the disc luminosity L_{disc} , on the fraction of the photons reflected from BLR ($\tau = 0.1$) and on the radius of BLR (R_{BLR}) for which a relation of $R_{\text{BLR}} = 10^{17} (L_{\text{disc}} / 10^{45}) \text{ cm}$ is assumed [38]. The disc luminosity is constrained by fitting a blackbody to the UV excess (Fig.2), which is likely caused by direct thermal emission from the accretion disc.

Using the observed data, additional constraints on the model parameters can be derived. For example, knowing the variability, the limit on the blob radius can be imposed from the relation $R \leq \delta ct / (1 + z) = 6.3 \cdot 10^{16} \text{ cm}$. Also, knowing the peak of the low and high energy components, additional constraints on the magnetic field and blob radius can be derived. All the parameters constrained from the observations are given as initial values for the parameter search, and through *minuit* optimization parameters best describing the data are obtained².

3.2. Modeling results. The SED modeling results are shown in Fig.2. The radio data are treated as upper limits during the modeling, as the emission in this band is produced from the low-energy electrons, which can propagate longer and are perhaps from more extended regions. Initially, the SED is modeled assuming that only synchrotron photons are inverse Compton up-scattered to higher energies, neglecting the external photons (solid line in Fig.2 upper panel). As the

² The fit is done using *jetset* package (<https://jetset.readthedocs.io/en/latest/>).

X-ray data are defining the low-energy tail of the SSC components, it allows to estimate $\alpha = 1.48$. For a softer power-law index of electrons, the rising shape of the X-ray data cannot be reproduced. The cut-off energy of electrons is $\gamma_{cut} = 5138.4$ well defined by the peak of the HE component. The minimum energy of the electrons was estimated to be at $\gamma_{min} = 7.34$, and the magnetic field $B = 44.8$ mG to have an energy density of $U_B = 8.0 \cdot 10^{-5}$ erg cm⁻³. The modeling also allows to estimate the jet power in the form of the magnetic field and electron kinetic energy, calculated by $L_B = \pi c R_b^2 \Gamma^2 U_B$ and $L_e = \pi c R_b^2 \Gamma^2 U_e$, respectively. The jet power in electrons is and that in the magnetic field is $1.05 \cdot 10^{46}$ erg s⁻¹. The jet is strongly particle dominated, required to explain the dominance of the HE component.

The results of the SED modeling when both internal and external photons are considered (SSC+EIC) is shown in Fig.2 (lower panel). The direct disc emission peaking at UV band (dashed line) is shown with a blackbody luminosity $4.7 \cdot 10^{46}$ erg s⁻¹ found by data fitting. In this case, the IC scattering of the synchrotron photons explains the observed X-ray flux while the γ -ray data are due to IC up-scattering of BLR photons. Since the averaged energy of BLR reflected photons exceeds the synchrotron ones, this results in lower cut-off energy of the electrons $\gamma_{cut} = 694.6$. In this case, again the X-ray data (at least lower part) are modeled by SSC which defines the power-law index of the electrons $\alpha = 1.95$. We note that a harder power-law index will better explain the hard X-ray data but it will increase also the energy of electrons and the predicted emission in the γ -ray band will overshoot the observed γ -ray data. The estimated magnetic field $B = 0.81$ G is higher than in the case of pure SSC modeling yielding to $U_e/U_B = 28$, which makes the system closer to the equipartition condition ($U_e/U_B = 1$). The jet energy carried by particles (electrons) and the magnetic field corresponds to $1.55 \cdot 10^{45}$ erg s⁻¹ and $5.51 \cdot 10^{43}$ erg s⁻¹, respectively.

4. Discussion and Conclusion. We report on the results of the multiwavelength observations of PKS 0537-286. Being among the most distant blazars observed in the γ -ray band ($z = 3.1$), PKS 0537-286 is an interesting target not only for investigating the physics of blazars in general but also it can provide information on the environment of supermassive black holes in the early Universe.

Swift XRT observations of PKS 0537-286 in different years show that its X-ray emission is nearly constant, changing in a narrow interval of $F_{X\text{-ray}} = (3.01 - 4.58) \cdot 10^{-12}$ erg cm⁻² s⁻¹. The X-ray emission is characterized by a remarkably hard photon index, $\Gamma_{X\text{-ray}} \leq 1.3$ which indicates that the second component in the SED, although having a peak below the γ -ray band, energetically dominates. In the Swift UVOT observations, all filters are not always available which prevents detailed variability studies in the optical band. In the available filters, the flux was estimated to be of the order of $\approx 10^{-12}$ erg cm⁻² s⁻¹ which is the same order as the reported archival flux of PKS 0537-286.

Though its large distance (26.9 Gpc), PKS 0537-286 is a bright source in the γ -ray band. Its averaged γ -ray spectrum is best described with a log-parabolic model with $\alpha = 2.70 \pm 0.0$, $\beta = 0.09 \pm 0.03$ and $F_\gamma = (4.19 \pm 0.15) \cdot 10^{-8}$ photon $\text{cm}^{-2} \text{s}^{-1}$. The temporal analyses of the γ -ray data show that the source is variable both in short and long time scales. For example, during a week around MJD 57874, the source flux significantly increased up to $(6.23 \pm 0.56) \cdot 10^{-7}$ photon $\text{cm}^{-2} \text{s}^{-1}$ with a photon index of 2.53 ± 0.09 . Using the distance of PKS 0537-286, the averaged flux corresponds to $L_\gamma = 1.44 \cdot 10^{48}$ erg s^{-1} which increases to $L_\gamma = 2.46 \cdot 10^{49}$ erg s^{-1} during the flare. Yet, considering $\delta = 20$, the total power emitted in the γ -ray band in the proper frame of the jet is $L_{em,\gamma} = L_\gamma / 2\delta^2 = 1.8 \cdot 10^{45}$ erg s^{-1} during the quiescent state and $L_{em,\gamma} = 3.1 \cdot 10^{46}$ erg s^{-1} during the flare.

The multiwavelength SED of PKS 0537-286 was modeled within one-zone synchrotron/SSC and SSC+EIC scenarios. When only the synchrotron photons are considered for the IC scattering, the data can be reproduced when the energy distribution of the emitted nonthermal electrons has a hard power-law index $\alpha = 1.48$ which extends up to $\gamma_{cut} = 5138.4$. As the second peak energetically dominates, the emission region in the jet should be strongly particle dominated $U_e/U_B = 2.4 \cdot 10^4$ and the total luminosity of the jet $\approx 10^{46}$ erg s^{-1} be carried by the particles. Alternatively, when the contribution from BLR reflected photons is considered, the required parameters are more relaxed. For example, $\alpha = 1.95$, and $\gamma_{cut} = 694.6$ the system is not far from the equipartition condition $U_e/U_B = 28$. This modeling has an advantage considering the required total jet power (the total luminosity of the jet is $\approx 1.60 \cdot 10^{45}$ erg s^{-1}) but it fails to well reproduce the observed hard X-ray data. We note, however, that the luminosity estimated in the previous case is well within the range of luminosities usually estimated for FSRQs.

The multiwavelength studies of distant blazar PKS 0537-286 show that it is a powerful emitter in the X-ray and γ -ray bands. The integrated luminosity of these components exceeds that of the low-energy component (from radio to optical bands). Through theoretical modeling of the SED several parameters were constrained which allowed a quantitative evaluation of the source parameters/properties. Considering the significant number (>100) of high redshift blazars ($z > 2.0$) detected in the HE γ -ray band, their detailed multiwavelength study can shed light on the understanding of the objects in the distant Universe.

Acknowledgements. This work was supported by the RA MES State Committee of Science, in the frames of the research project No 18T-1C335. This work used resources from the ASNET cloud and the EGI infrastructure with the dedicated support of CESGA (Spain).

¹ ICRANet Armenia Marshall Baghramian Avenue 24a, 0019 Yerevan, Armenia, e-mail: narsahakyan@gmail.com

² ICRANet Piazza della Repubblica 10, 65122 Pescara, Italy

МНОГОВОЛНОВОЕ ИЗУЧЕНИЕ ДАЛЕКОГО БЛАЗАРА PKS 0537-286

Н.СААКЯН^{1,2}, Д.ИСРАЕЛЯН¹, Г.АРУТЮНЯН¹

Представлены результаты многоволновых наблюдений далекого блазара PKS 0537-286 ($z = 3.1$). Используются данные, накопленные в течение более чем десяти лет телескопом Fermi-LAT вместе с архивными данными Swift UVOT/XRT, за период 2005-2017гг. В γ -диапазоне выше 100 МэВ максимальный поток был зарегистрирован 30.04.2017 в течение одной недели $F_\gamma = (6.23 \pm 0.56) \cdot 10^{-7}$ photon cm⁻² s⁻¹, что соответствует $L_\gamma = 2.46 \cdot 10^{49}$ эрг с⁻¹ изотропной светимости. Анализ данных Swift XRT показывает, что рентгеновое излучение характеризуется значительно жестким фотонным индексом $\Gamma_{X\text{-ray}} \leq 1.3$, а его поток составляет $\approx 4 \cdot 10^{-12}$ эрг см⁻² с⁻¹, оставаясь почти постоянным на протяжении двенадцати лет. Спектральное распределение энергии моделирована в рамках однозонной лептонной модели, при предположении, что область излучения находится в области широкой линии. Наблюдаемые рентгеновские и данные моделированы с привлечением обратного комптоновского рассеяния а) только синхротронных фотонов и б) синхротронных и внешних фотонов на популяции электронов, которая излучает от радио до оптического диапазона. Моделирование показывает, что а) в струе со светимостью между 10^{45} - 10^{46} эрг с⁻¹ должны доминировать частицы, б) нетепловые электроны в струе PKS 0537-286 имеют жесткий степенной индекс (< 1.9).

Ключевые слова: *PKS 0537-286: γ -излучение: блазары*

REFERENCE

1. Fermi-LAT collaboration, arXiv e-prints, arXiv:1902.10045, 2019.
2. N.Sahakyan, V.Baghmanyany, D.Zargaryan, Astron. Astrophys., **614**, A6, 2018.
3. N.Sahakyan, D.Zargaryan, V.Baghmanyany, Astron. Astrophys., **574**, A88, 2015.
4. D.Zargaryan, S.Gasparyan, V.Baghmanyany et al., Astron. Astrophys., **608**, A37, 2017.
5. V.Baghmanyany, S.Gasparyan, N.Sahakyan, Astrophys. J., **848**, 111, 2017.
6. V.Baghmanyany, N.Sahakyan, IJMPD, **27**, 1844001, 2018.
7. C.M.Urry, P.Padovani, Publ. Astron. Soc. Pacif., **107**, 803 1995.
8. L.Foschini, G.Bonnoli, G.Ghisellini et al., Astron. Astrophys., **555**, A138, 2013.

9. *B.Rani, B.Lott, T.P.Krichbaum et al.*, *Astron. Astrophys.*, **557**, A71, 2013.
10. *M.Ackermann, R.Anantua, K.Asano et al.*, *Astrophys. J. Lett.*, **824**, L20, 2016.
11. *M.Aartsen, M.Ackermann, J.Adams*, *Science*, **361**, 1378, 2018.
12. *M.Aartsen, M.Ackermann, J.Adams*, *Science*, **361**, 147, 2018.
13. *P.Padovani, P.Giommi, E.Resconi et al.*, *Mon. Not. Roy. Astron. Soc.*, **480**, 192, 2018.
14. *S.Ansoldi, L.A.Antonelli, C.Arcaro et al.*, *Astrophys. J.*, **863**, L10, 2018.
15. *M.Cerruti, A.Zech, C.Boisson et al.*, *Mon. Not. Roy. Astron. Soc.*, **483**, L12, 2019.
16. *S.Gao, A.Fedynitch, W.Winter et al.*, *Nature Astron.*, **3**, 88, 2019.
17. *N.Sahakyan*, *Astrophys. J.*, **866**, 109, 2018.
18. *N.Sahakyan*, *Astron. Astrophys.*, **622**, A144, 2019.
19. *A.Abdo, M.Ackermann, M.Ajello et al.*, *Astrophys. J.*, **736**, 131, 2011.
20. *S.Gasparyan, N.Sahakyan, V.Baghmanyant et al.*, *Astrophys. J.*, **863**, 114, 2018.
21. *N.Sahakyan, S.Gasparyan*, *Mon. Not. Roy. Astron. Soc.*, **470**, 2861, 2017.
22. *M.Hayashida, K.Nalewajko, G.Madejski et al.*, *Astrophys. J.*, **807**, 79, 2015.
23. *M.Sikora, L.Stawarz, R.Moderski et al.*, *Astrophys. J.*, **704**, 38, 2009.
24. Fermi-LAT collaboration, arXiv e-prints, arXiv:1905.10771, 2019.
25. *M.Cappi, M.Matsuoka, A.Comastri et al.*, *Astrophys. J.*, **478**, 492, 1997.
26. *F.Fiore, M.Elvis, P.Giommi et al.*, *Astrophys. J.*, **492**, 79, 1998.
27. *J.N.Reeves, M.Turner, P.Bennie et al.*, *Astron. Astrophys.*, **365**, L116, 2001.
28. *N.Gehrels et al.*, *Astrophys. J.*, **611**, 1005, 2004.
29. *W.Cash*, *Astrophys. J.*, **228**, 939, 1979.
30. *T.Poole, A.Breeveld, M.Page et al.*, *Mon. Not. Roy. Astron. Soc.*, **383**, 627, 2008.
31. *W.B.Atwood, A.A.Abdo, M.Ackermann et al.*, *Astrophys. J.*, **697**, 1071, 2009.
32. *E.Massaro, M.Perri, P.Giommi et al.*, *Astron. Astrophys.*, **413**, 489, 2004.
33. *L.Maraschi, G.Ghisellini, A.Celotti*, *Astrophys. J.*, **397**, L5, 1992.
34. *S.D.Bloom, A.P.Marscher*, *Astrophys. J.*, **461**, 657, 1996.
35. *G.Ghisellini, L.Maraschi, A.Treves*, *Astron. Astrophys.*, **146**, 204, 1985.
36. *M.Sikora, M.Begelman, M.Rees*, *Astrophys. J.*, **421**, 153, 1994.
37. *M.Biazejewski, M.Sikora, R.Moderski et al.*, *Astrophys. J.*, **545**, 107, 2000.
38. *G.Ghisellini, F.Tavecchio*, *Mon. Not. Roy. Astron. Soc.*, **397**, 985, 2009.